JACS
JOURNAL OF THE AMERICAN CHEMICAL SOCIETY
Article
pubs.acs.org/JACS

A New Direction in Dye-Sensitized Solar Cells Redox Mediator Development: In Situ Fine-Tuning of the Cobalt(II)/(III) Redox Potential through Lewis Base Interactions

Muhammad K. Kashif,[†] Jordan C. Axelson,[‡] Noel W. Duffy,[§] Craig M. Forsyth,[⊥] Christopher J. Chang,[¶] Jeffrey R. Long,[‡] Leone Spiccia,*[,⊥] and Udo Bach*[,†,#,&]

[†]Department of Materials Engineering, Monash University, Victoria 3800, Australia

[‡]Department of Chemistry, University of California, Berkeley, California 94720-1460, United States

[§]Commonwealth Scientific and Industrial Research Organization, Energy Technology, Clayton South, Victoria 3169, Australia

[⊥]School of Chemistry, Monash University, Victoria 3800, Australia

[¶]Department of Chemistry and the Howard Hughes Medical Institute, University of California, Berkeley, California 94720-1460, United States, and Chemical Sciences Division, Lawrence Berkeley National Laboratory, Berkeley, California, 94720, United States

[#]Commonwealth Scientific and Industrial Research Organization, Materials Science and Engineering, Clayton South, Victoria 3169, Australia

[&]Melbourne Centre for Nanofabrication, 151 Wellington Road, Clayton, Victoria 3168, Australia

Supporting Information

ABSTRACT: Dye-sensitized solar cells (DSCs) are an attractive renewable energy technology currently under intense investigation. In recent years, one area of major interest has been the exploration of alternatives to the classical iodide/triiodide redox shuttle, with particular attention focused on cobalt complexes with the general formula $[Co(L)_n]^{2+/3+}$. We introduce a new approach to designing redox mediators that involves the application of $[Co(PY5Me_2)(MeCN)]^{2+/3+}$ complexes, where $PY5Me_2$ is the pentadentate ligand, 2,6-bis(1,1-bis(2-pyridyl)ethyl)pyridine. It is shown, by X-ray crystallography, that the axial acetonitrile (MeCN) ligand can be replaced by more strongly coordinating Lewis bases (B) to give complexes with the general formula $[Co(PY5Me_2)(B)]^{2+/3+}$, where B = 4-*tert*-butylpyridine (tBP) or *N*-methylbenzimidazole (NMBI). These commonly applied DSC electrolyte components are used for the first time to fine-tune the potential of the redox couple to the requirements of the dye through coordinative interactions with the $Co^{II/III}$ centers. Application of electrolytes based on the $[Co(PY5Me_2)(NMBI)]^{2+/3+}$ complex in combination with a commercially available organic sensitizer has enabled us to attain DSC efficiencies of 8.4% and 9.2% at a simulated light intensity of 100% sun (1000 W m^{-2} AM1.5 G) and at 10% sun, respectively, higher than analogous devices applying the $[Co(bpy)_3]^{2+/3+}$ redox couple, and an open circuit voltage (V_{oc}) of almost 1.0 V at 100% sun for devices constructed with the tBP complex.

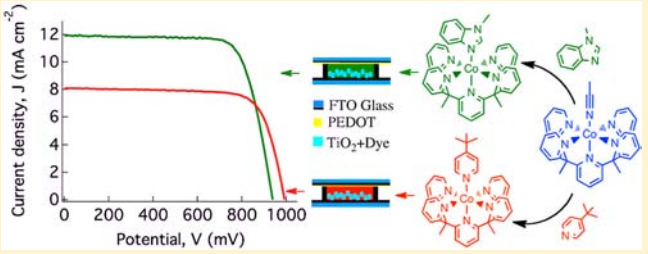

INTRODUCTION

The ever-increasing energy demands and concerns over climate change are motivating scientists to tackle present and future energy challenges. Dye-sensitized solar cells (DSCs) are considered to be a promising green technology capable of meeting our future energy demands. The unique design of DSCs offers a wide range of choices for its components, such as nanocrystalline metal oxides, photosensitizers, counter electrode materials, redox mediators, and electrolytes. In these devices, upon optical excitation of the photosensitizer and subsequent electron injection into the nanocrystalline metal oxide, the redox mediator present in the electrolyte regenerates the photosensitizer. The redox mediator not only ensures efficient dye regeneration but also transports positive charge to the catalyst-coated counter electrode. Lewis bases, such as 4-*tert*-butylpyridine (tBP) and less commonly *N*-methylbenzimidazole (NMBI), have been used as additives in the electrolyte.[1−3] The resultant increase in the efficiency of DSC performance upon addition of these Lewis bases has been attributed to the negative shift of the titania conduction band edge as well as to a reduction in the rates of interfacial charge recombination reactions.[4−9] Periodic density-functional calculations have also shown that adsorbate molecules with nitrogen donor atoms induce a negative shift of the TiO_2 conduction band edge.[10]

Until recently, iodide/triiodide (I^-/I_3^-) was the redox mediator of choice for the construction of highly efficient

Received: June 18, 2012
Published: September 11, 2012

dx.doi.org/10.1021/ja305897k | J. Am. Chem. Soc. 2012, 134, 16646−16653

DSCs. Recognition of the need to address some of the shortcomings of this redox couple, such as incompatibility with metallic conductors and a significant loss in energy arising from the large driving force required for the regeneration of the photooxidized dye, is now stimulating interest in new redox mediators.[11−21] Of all the alternatives examined thus far, $Co^{II/III}$ polypyridyl redox couples have emerged as leading candidates to replace the I^-/I_3^- redox shuttle.[22−29] $Co^{II/III}$ complexes are generally noncorrosive toward most metals, and modification in the ligand architecture can be used to fine-tune the $Co^{II/III}$ redox potential so as to achieve efficient dye regeneration and at the same time maximize the open circuit potential (V_{OC}).[19,24] The advantage of these redox mediators was recently demonstrated by the use of the $[Co(bpy)_3]^{2+/3+}$ couple in DSCs, which achieved a record efficiency of 12.3% and V_{OC} of 965 mV.[30]

A large inner-sphere reorganization energy in the cases of $[Co(bpy)_3]^{2+/3+}$ and $[Co(phen)_3]^{2+/3+}$ has been suggested to result in slow rates of interfacial recombination between photoinjected electrons and the Co^{III} complexes, thus leading to high efficiencies.[31−34] In a further recent development, a cobalt complex of formula $[Co(L^1)_2]^{2+/3+}$, where L^1 is the tridentate ligand [6-(1*H*-pyrazol-1-yl)-2,2′-bipyridine)], achieved a high V_{OC} of 998 mV and an impressive efficiency of 10%.[19]

The denticity and spatial arrangement of the donor atoms are features of a ligand that can be manipulated to design metal complexes with particular properties and coordination geometries. In addition to the electron-donating properties of the ligands, the rigidity and number of donor atoms are important in determining the stability and electrochemical properties of a particular complex. Moreover, the ligand properties can be used to modulate the relative activation energies for electron-transfer processes involving the metal complexes.

Here, we report a new approach to designing redox mediators, which exploits the coordination properties of Lewis bases commonly added to DSC electrolyte solutions. The pair of cobalt complexes chosen for this purpose have the formula $[Co(PY5Me_2)(MeCN)](OTf)_2$ (**1a**) and $[Co(PY5Me_2)(MeCN)](TFSI)_3$ (**1b**) ($PY5Me_2$ = (2,6-(bis(bis-2-pyridyl)methylmethane)pyridine, see Scheme 1). The nitrogen donors in the pentadentate polypyridyl ligand, $PY5Me_2$, occupy the corners of a square-pyramid when bound to the metal center. In complexes **1a**/**1b**, the sixth coordination site of the octahedral ligand field is occupied by a weakly bound acetonitrile (MeCN) molecule, which can be readily replaced by more strongly binding ligands. This feature provides an opportunity to fine-tune the potential of the $Co^{II/III}$ redox couple through the addition of suitable strongly coordinating Lewis bases to form complexes of composition $[Co(PY5Me_2)(B)](OTf)_2$ (see Scheme 1). Furthermore, we examined whether the introduction of the chelating pentadentate ligand offers advantages in terms of the key electron transfer processes occurring in DSCs.

We describe the synthesis and characterization of two pairs of $[Co(PY5Me_2)(B)]^{2+/3+}$ complexes, where B corresponds to tBP (**2a**/**2b**) and NMBI (**3a**/**3b**), two bases commonly used as additives in DSC electrolytes, and the application of these complexes as redox mediators in DSCs using the D-π-A organic dye, MK2 (2-cyano-3-[5‴-(9-ethyl-9H-carbazol-3-yl)-3′,3″,3‴,4-tetra-*n*-hexyl-[2,2′,5′,2″,5″,2‴]-quarter thiophen-5-yl] acrylic acid) (see Figure 1). The exciting finding to emerge from this study is the significantly improved efficiency of DSCs constructed with the NMBI complex in comparison to the efficiencies obtained when using the tBP analogue or $[Co(bpy)_3]^{2+/3+}$ complex.

Scheme 1. Shown are the 1a, 2a and 3a Cations for the Co^{II} Complexes and the 1b, 2b and 3b Cations for the Co^{III} Complexes[a]

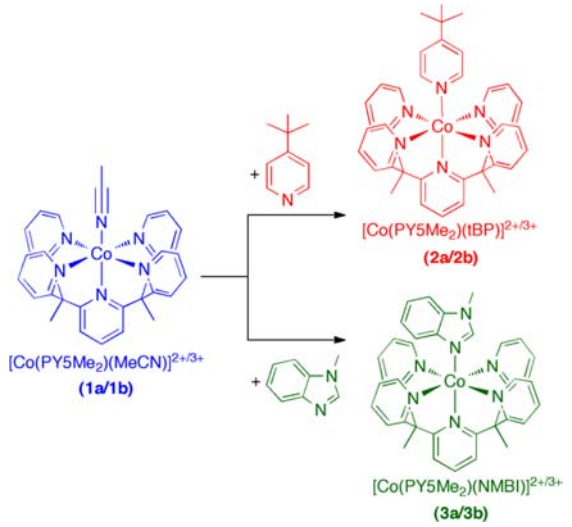

[a]The syntheses are described in the Experimental Section.

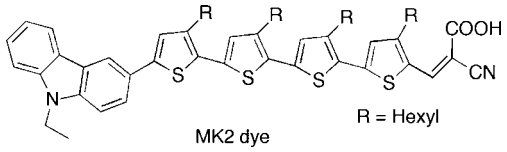

Figure 1. Structure of the MK2 dye.

EXPERIMENTAL SECTION

Materials and Methods. All general reagents and solvents were obtained from commercial sources. Anhydrous solvents were stored in the glovebox. The compounds MK2, bpy (2,2′-bipyridine), tBP (4-*tert*-butylpyridine), NMBI (*N*-methylbenzimidazole), LiTFSI (lithium bis(trifluoromethane)sulfonimide), EDOT (3,4-ethylenedioxythiophene), MeCN and other solvents were purchased from Sigma Aldrich. AgTFSI (silver bis(trifluoromethane)sulfonimide), AgOTf (silver trifluoromethansulfonate) and $NOBF_4$ were purchased from Strem Chemicals Inc. TiO_2 nanoparticles (Ø 30 and 400 nm particles) were obtained from JGC Catalysts and Chemicals Ltd. ^1H and ^{19}F NMR spectra were measured on a Bruker DRX 400 spectrometer, using the signal of the deuterated solvent as an internal standard. The chemical shifts δ are reported in parts per million (ppm) relative to tetramethylsilane (TMS). The values of coupling constants (J) are given in Hertz (Hz). Peak multiplicities are abbreviated as follows: s (singlet), d (doublet), t (triplet), and m (multiplet). Microanalyses were carried out by the Campbell Microanalytical Laboratory, University of Otago, New Zealand. UV−visible spectra were recorded with a Lambda 950 Perkin-Elmer spectrophotometer. All electrochemistry experiments were performed at 22 °C in a three-electrode cell joined to a VSP workstation. The reference electrode was a CH Instruments $Ag/AgNO_3$ nonaqueous electrode. $Fc^{0/+}$ was used as a reference system and a conversion factor of 635 mV was used to convert electrochemical potential vs ferrocene to NHE.

Synthesis of the Cobalt Complexes. Unless otherwise noted, all synthetic procedures as well as electrolyte filling of the DSCs were performed under inert N_2 atmosphere, using standard glovebox techniques. The ligand $PY5Me_2$ was synthesized as previously described.[35] The complex $[Co(PY5Me_2)(MeCN)](OTf)_2$ (**1a**) was

dx.doi.org/10.1021/ja305897k | J. Am. Chem. Soc. 2012, 134, 16646−16653

obtained with use of the method of Zadrozny et al.,[36] but substituting AgOTf for $TlPF_6$.

*[Co(PY5Me$_2$)(tBP)](OTf)$_2$·2MeCN (**2a**).* This compound was accessed by the addition of tBP (6.8 mg, 0.050 mmol) into a stirred mixture of **1a** (42 mg, 0.050 mmol) in 10 mL of acetonitrile, at room temperature. Compound **1a** is very poorly soluble in acetonitrile. However, it becomes soluble upon addition of tBP. The solution was stirred for 1 h at room temperature to ensure ligand exchange was complete. Layering with Et_2O induced crystallization. Yield: 45 mg (96%) of **2a** as pink crystals. Crystals of the diacetonitrile solvate suitable for X-ray diffraction analysis were obtained by the diffusion of Et_2O into a concentrated acetonitrile solution of **2a**. Elemental analysis: Found (Calcd) for $C_{42s}H_{41}CoF_6N_7O_6S_2$ (**2**): C, 51.64 (51.34); H, 4.23 (4.09); N, 8.74 (8.98).

*[Co(PY5Me$_2$)(NMBI)](OTf)$_2$·2MeCN. (**3a**).* Compound **3a** was prepared by the addition of NMBI (6.6 mg, 0.050 mmol) into an acetonitrile mixture of **1a** (42 mg, 0.050 mmol) following the procedure described for compound **2a**. Yield: 43 mg (95%) of **3a** as pink crystals. Crystals of the diacetonitrile solvate suitable for X-ray diffraction analysis were obtained by the diffusion of Et_2O into an acetonitrile solution of **3a**. Elemental analysis: Found (Calcd) for $C_{39}H_{33}CoF_6N_7O_6S_2$ (**3**): C, 49.98 (50.22); H, 3.66 (3.57); N, 11.14 (10.51).

*[Co(PY5Me$_2$)(MeCN)](TFSI)$_3$ (**1b**), [Co(PY5Me$_2$)(tBP)](TFSI)$_3$ (**2b**), and [Co(PY5Me$_2$)(NMBI)](TFSI)$_3$·3CH$_2$Cl$_2$ (**3b**).* The synthesis of **2b** and **3b** followed a similar procedure to that described for **2a** and **3a**. However, high-quality crystals could not be grown for complexes **2b** and **3b** when $NOBF_4$ was used as the oxidant. In addition, following oxidation of the Co^{II} complex to the corresponding Co^{III} complex with use of $NOBF_4$ it was found that the BF_4^- slowly decomposes generating fluoride ions, which then coordinate to the Co^{III} center. Hence, AgTFSI was used as the oxidant and the products isolated as TFSI salts. To prepare **1b** solid AgTFSI (35 mg, 0.13 mmol) and **1a** (34 mg, 0.043 mmol) were added to 10 mL of CH_2Cl_2 and the mixture was stirred for 1 h, giving a light orange mixture containing Ag particles, which were removed by filtration through diatomaceous earth. Orange crystals of [Co(PY5Me$_2$)(MeCN)](TFSI)$_3$·3(CH$_2$Cl$_2$) (**1b**) were obtained by layering with Et_2O. Yield: 45 mg (75%) as orange crystals. **1b** was then reacted (as described for **2a** and **3a**) with tBP and NMBI to give **2b** and **3b**, respectively. A high yield (97%) was obtained for complexes **2b** and **3b.** Crystals of [Co(PY5Me$_2$)(NMBI)](TFSI)$_3$·3CH$_2$Cl$_2$ (**3b**) suitable for X-ray diffraction studies were obtained by vapor diffusion of Et_2O into a concentrated solution of **3b** in acetonitrile. Despite numerous attempts, crystals of **2b** suitable for X-ray crystallography could not be obtained.

[Co(PY5Me$_2$)(tBP))](TFSI)$_3$ (**2b**): ^{1}H NMR (400 MHz, CD_3CN, 22 °C) δ 9.63 (d, J_{HH} = 8 Hz, 4H, py-H), 8.35−8.32 (m, 1 H, py-H), 8.30−8.24 (m, 6 H, py-H), 8.18−8.16 (M, 4H, py-H), 8.07−8.04 (m, 1H, tBP-H), 7.97−7.95 (m, 1H, tBP-H), 7.90−7.87 (m, 4H, py-H), 7.72−7.68 (m, 2H, tBP-H), 5.47 (s, 9H, tBP-3CH$_3$), 2.96−2.81 (m, 6H, Me$_2$−H).

[Co(PY5Me$_2$)(NMBI))](TFSI)$_3$ (**3b**): ^{1}H NMR (400 MHz, CD_3CN, 22 °C) δ 9.67 (m, 1H, NMBI-H), 8.81 (d,, J_{HH} = 8 Hz, 2 H, NMBI-H), 8.57 (d,, J_{HH} = 8 Hz, 2 H, NMBI-H), 8.37−8.16 (m, 11 H, py-H), 8.01−7.90 (m, 2H, py-H), 7.70−7.60 (m, 2 H, py-H), 7.56−7.52 (m, 1 H, py-H), 7.37−7.34 (m, 2 H, py-H), 6.85 (s, 1 H, py-H), 4.05−3.94 (m, 3 H, CH$_3$−NMBI), 3.01−2.98 (m, 6 H, Me$_2$−H).

Data Collection. Representative orange or orange-red prismatic crystals of **2a**, **3a**, and **3b** were mounted on an Oxford Gemini Ultra CCD diffractometer equipped with an Oxford Cryosystems 700 Cryostream and cooled to 123(1) K. Data were collected with Mo Kα radiation (λ = 0.71073 Å) and processed with CrysAlisPro software; Lorentz, polarization, and absorption corrections (multiscan) were applied. The structures were solved and refined with SHELX-97.[37] All non-hydrogen atoms were refined with anisotropic thermal parameters and hydrogen atoms were placed in calculated positions, using a riding model with C−H = 0.95−0.98 Å and U_{iso}(H) = xU_{iso}(C), x = 1.2 or 1.5. For **3a**, one of the CF_3SO_3 counterions was modeled as disordered with the CF_3 and SO_3 groups each occupying two positions rotated by approximately 15° about the S−C bond. The disordered atoms were refined with occupancies fixed at 0.5, with equivalent C−F and S−O distances restrained to be the same and with the anisotropic thermal parameters for some atoms restrained to be similar. A summary of crystallographic data can be found in Table 1.

Table 1. Crystallographic Data for 2a, 3a, and 3b

	2a	3a	3b
formula	$C_{44}H_{44}CoF_6N_8O_6S_2$	$C_{43}H_{39}CoF_6N_9O_6S_2$	$C_{46}H_{39}Cl_6CoF_{18}N_{10}O_{12}S_6$
fw	1017.94	1014.88	1729.86
crystal system	monoclinic	triclinic	triclinic
space group	$P2_1/c$	$P\bar{1}$	$P\bar{1}$
a (Å)	14.4264(9)	12.5214(7)	13.4281(6)
b (Å)	14.7665(11)	13.0143(11)	13.7502(5)
c (Å)	21.3870(14)	15.4881(8)	19.9835(9)
α (deg)	90	108.227(6)	74.802(4)
β (deg)	93.340(6)	90.845(4)	87.534(4)
γ (deg)	90	113.083(7)	66.118(4)
V (Å^3)	4548.3(5)	2177.9(2)	3247.5(2)
Z	4	2	2
μ_{calcd} (mm^{-1})	0.551	0.576	0.821
ρ_{calcd} (g·cm^{-1})	1.487	1.548	1.769
2θ range (deg)	3.96−55.0	3.74−64.70	3.82−60.0
N_t	26161	28652	40980
$N(R_{int})$	10440 (0.057)	14035 (0.051)	18933 (0.033)
N_o	8023	9473	13918
$R1$ ($I > 2\sigma I$)	0.056	0.059	0.058
wR ($I > 2\sigma I$)	0.143	0.137	0.136
R(all data)	0.076	0.094	0.086
wR(all data)	0.159	0.164	0.167
GoF	1.051	1.037	1.027
$\Delta\rho_{max/min}$ (e)	1.05; −0.82	1.20; −1.05	1.74; −1.32

Device Fabrication. Established procedures were followed for DSC fabrication.[12] A 1 μm thick film (4 × 4 mm) of 30 nm-sized TiO_2 particles was screen printed on fluorine-doped SnO_2 (FTO) conducting glass electrodes (4 mm thick and 10 Ω/□). A second layer was printed by using 400 nm-sized particles to produce a titania layer with overall thickness of 3 μm. A 2 μm thick transparent TiO_2 film (4 × 4 mm) with 30 nm-sized TiO_2 particles was deposited for the IMVS-IMPS studies. Following the application of a first sintering process (500 °C) to the screen-printed films, a $TiCl_4$ treatment was carried out by submerging the films in an aqueous solution containing 40 mM $TiCl_4$ at 70−75 °C. After heating the films with a heat gun at 570 ± 25 °C for 40 min, the films were immersed for 6 h in a 0.2 mM solution of MK2 in an acetonitrile:toluene (1:1) mixture. The PEDOT counter electrodes were prepared by electropolymerizing EDOT on the FTO substrate.[38] Working electrode and counter electrode were bonded together with a 25 μm thick hot melt Surlyn gasket. Electrolytes were filled into the space between the two electrodes by using a backfilling technique under vacuum. The electrolyte-injecting hole was sealed with hot melt Surlyn backed by aluminum foil.

IV and IPCE Instrumentation. An Oriel sun simulator equipped with a filtered 1000 W xenon lamp was used as a source of simulated solar irradiation (AM 1.5 G, 1000 W/m^2). A calibrated silicon photodiode provided by Peccell Technologies was used to adjust the output of the light source and a color filter was used to minimize the optical mismatch between the calibration diode and the DSCs. The IV characteristics of the cells under these conditions were recorded with use of a Keithley 2400 source meter. Light intensities below one sun were achieved by using a filter wheel fitted with a series of mesh filters. Incident photon conversion efficiency was measured by an Oriel system fitted with a 150 W xenon lamp, linked to a Cornerstone 260

dx.doi.org/10.1021/ja305897k | J. Am. Chem. Soc. 2012, 134, 16646−16653

monochromator. IPCE photocurrents of the DSCs were recorded under short circuit conditions by means of a Keithley 2400 source meter. The monochromatic photon flux was quantified by using a calibrated silicon photodiode (Peccell Technologies).

Intensity Modulated Photovoltage Spectroscopy, Intensity Modulated Photocurrent Spectroscopy (IMVS-IMPS) and Charge Extraction Instrumentation. IMVS-IMPS studies were carried out on complete DSCs by using a combination of red and white light LEDs. The light intensity of the red LED powered by an adjustable DC voltage source was modulated to a depth of 2% by the integral function generator of a Stanford lock-in-amplifier (SR810). The lock-in-amplifier is capable of providing a sine wave modulation between 0.1 Hz and 30 kHz. To achieve one sun equivalent, an additional white light diode array controlled by a commercial DC power source was used. All experiments were carried out in an earthed Faraday dark box to remove electrical noise at low light intensities. The photovoltage was recorded with the help of a high impedance voltage follower (input impedance 10^{12} Ω), powered by a battery. The amplitude and phase of the resulting AC photovoltages were captured by using the lock-in amplifier run under a computer-controlled program Labview. A fitting program written in Labview was used for the data analysis. An unmodulated white light illuminated the DSC for 10 s to attain equilibrium between charge injection and recombination under open circuit conditions. An integrated computer-controlled mercury-wetted relay switch was used to switch the light off and to put the device to short circuit. The resultant extracted charge was measured across a 50 Ω resistor, using an NI-6251 data logger.

RESULTS AND DISCUSSION

A key step in fine-tuning the redox potential of the $Co^{II/III}$ redox shuttle involved ligation of the Lewis bases to the parent complex **1a**. The complexes $[Co(PY5Me_2)(tBP)](OTf)_2$ (**2a**) and $[Co(PY5Me_2)(NMBI)](OTf)_2$ (**3a**) were accessed by the addition of tBP and NMBI, respectively, to an acetonitrile solution of **1a** (see Scheme 1). The axial MeCN ligand in **1a** is readily displaced by these more strongly binding monodentate ligands. The preparation of the Co^{III} complexes was achieved by first preparing $[Co(PY5Me_2)(MeCN)](TFSI)_3$, through oxidation of **1a** with AgTFSI, and then reacting the product with tBP and NMBI to afford $[Co(PY5Me_2)(tBP)](TFSI)_3$ (**2b**) and $[Co(PY5Me_2)(NMBI)](TFSI)_3$ (**3b**), respectively.

Crystallography. Single crystals of $[Co^{II}(PY5Me_2)(tBP)](OTf)_2\cdot 2MeCN$ (**2a**) and $[Co^{II}(PY5Me_2)(NMBI)](OTf)_2\cdot 2MeCN$ (**3a**) suitable for X-ray analysis were obtained on addition of tBP and NMBI to an acetonitrile solution of the Co^{II} complex **1a**, respectively. Similarly, $[Co(PY5Me_2)(NMBI)](TFSI)_3\cdot 3(CH_2Cl_2)$ (**3b**) was obtained by the addition of tBP to the trivalent analogue of complex **1a**. All three complexes display a distorted octahedral $Co^{II/III}$ geometry with either the tBP or NMBI ligands in the axial position (Figures 2 and S4, SI).

The coordination spheres for complexes **2a** and **3a** are very similar, with the Co−N_{Py} distances (see Table 2) in the range of 2.122(2)−2.156(1) Å (**2a**) and 2.108(2)−2.156(2) Å (**3a**). These bond lengths are marginally longer than those for the MeCN complex **1a** (2.095(3)−2.142(3) Å).[39] The Co−N_6 (*N*-atom of the base) distances of 2.122(3) (**1a**), 2.129(2) (**2a**), and 2.108(2) Å (**3a**) also show little difference. The longer Co−N_{Py} bond lengths in **2a** and **3a** are accompanied by a displacement of the Co atom out of the equatorial plane by 0.139(1) and 0.149(1) Å (cf., the Co in **3b** is coplanar with the four equatorial pyridyl donors, −0.037(1) Å). The ability of the $PY5Me_2$ ligand to absorb the structural effects arising from changes in the oxidation state of the central metal atoms (e.g., two-electron Mo^{II}−Mo^{IV} changes) has been previously established.[40] However, in the current structures, the shortening of the Co−N bonds from **3a** to **3b** results in an unusually close approach (1.81 Å for **3b** cf. 2.15 Å for **3a**) of two neighboring *o*-H atoms on the terminal pyridyl groups (Figures 2 and S4, SI). A top view of the complex cations of **2a**, **3a**, and **3b** shows a highly symmetrical alignment of the axial ligand (tBP and NMBI) and the Me_2C−PY_1−CMe_2 plane (see Figure S3, SI).

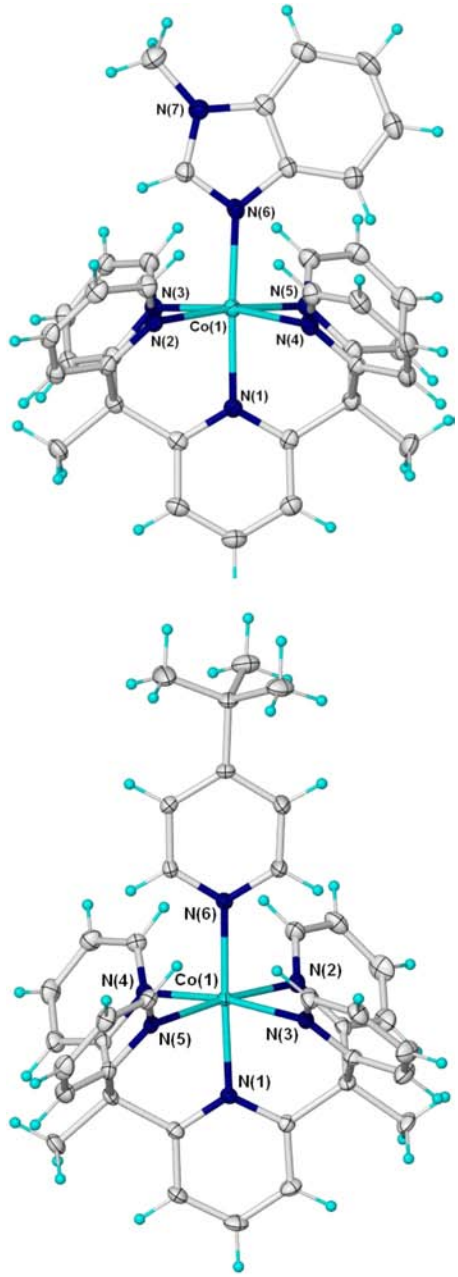

Figure 2. Crystal structures of the octahedral complexes $[Co(PY5Me_2)(tBP)]^{2+}$ (**2a** cation) and $[Co(PY5Me_2)(NMBI)]^{2+}$ (**3a** cation), with the pale blue, gray, and dark blue spheres representing Co, C, and N, respectively. Ellipsoids are depicted at the 50% probability level.

The Co−N bond lengths for $[Co(PY5Me_2)(NMBI)]^{2+}$ (**3a** cation) and $[Co(PY5Me_2)(NMBI)]^{3+}$ (**3b** cation) indicate that oxidation of the Co center results in an average decrease in the Co−N bond distances of 0.150(6) Å (calculated as the average difference in bond lengths for pairs of identical Co−N bonds in each complex). The corresponding change in bond distances

Table 2. Selected Bond Distances (Å) and Angles (deg) for 2a, 3a, and 3b

bond/angle	2a	3a	3b
Co−N(1)[a]	2.122(2)	2.122(2)	1.976(2)
Co−N(2)	2.132(2)	2.145(2)	1.989(2)
Co−N(3)	2.156(2)	2.156(2)	1.999(2)
Co−N(4)	2.145(2)	2.140(2)	1.999(2)
Co−N(5)	2.135(2)	2.140(2)	1.991(2)
Co−N(6)[b]	2.129(2)	2.108(2)	1.960(2)
N(1)−Co−N(6)	177.88(9)	177.26(8)	179.1(1)
N(2)−Co−N(5)	173.59(9)	172.61(8)	176.9(1)
N(3)−Co−N(4)	171.32(9)	170.87(8)	177.4(1)
N(2)−Co−N(4)	97.22(9)	99.11(8)	93.4(1)
N(5)−Co−N(3)	98.29(9)	96.48(8)	96.7(1)
N(3)−Co−N(2)	82.64(9)	80.21(8)	84.4(1)
N(5)−Co−N(4)	80.89(9)	83.10(8)	85.4(1)
N(1)−Co−N(3)	85.42(8)	86.26(8)	89.2(1)
N(1)−Co−N(2)	86.62(9)	87.12(8)	89.0(1)
N(1)−Co−N(4)	85.91(9)	84.61(8)	89.4(1)
N(1)−Co−N(5)	87.14(9)	86.07(7)	88.1(1)

[a]Axial $PY5Me_2$ pyridyl donor. [b]Axial Co−N(NMBI) bond.

for $[Co(bpy)_3]^{2+/3+}$ is 0.198(6) Å.[42,43] Thus, the constrained nature of the $PY5Me_2$ ligand appears to have a significant influence on the Co^{III} geometry. As a consequence, oxidation/reduction reactions involving the $[Co(PY5Me_3)(B)]^{2+/3+}$ complexes are likely to require less inner-sphere reorganization (vide infra).

Electrochemistry. The electrochemical properties of complexes **1a**−**3a** were investigated by using cyclic voltammetry under nitrogen. For compound **1a**, two quasi-reversible redox reactions are observed at half-wave potentials of $E_{1/2}$ = −0.845 V and +0.803 V vs NHE, corresponding to the $[Co(PY5Me_2)(MeCN)]^{1+/2+}$ and $[Co(PY5Me_2)(MeCN)]^{2+/3+}$ redox reactions, respectively (Figure S1a in the SI). This is consistent with previous literature reports.[36,39] Upon introduction of tBP and NMBI to form **2a** and **3a**, the $Co^{II/III}$ redox potential was lowered to a more negative value relative to that of **1a**. The $E_{1/2}$ for $[Co(PY5Me_2)(tBP)]^{2+/3+}$ shifted slightly to +0.780 V vs NHE, whereas $E_{1/2}$ for $[Co(PY5Me_2)(NMBI)]^{2+/3+}$ shifted to +0.714 V vs NHE (see Figure 3a). The corresponding redox potential for $[Co(bpy)_3]^{2+/3+}$ is 0.56 V vs NHE and is virtually unaffected by the addition of the bases. The redox potentials (vs NHE) derived for complexes **2a** and **3a**, $[Co(bpy)_3]^{2+/3+}$, and the HOMO LUMO levels of MK2 are compared in Figure 3b. These redox properties indicate that these complexes are well suited for DSC electrolyte development. The displacement of a monodentate ligand by an alternative Lewis base, which in turn affects the electrochemical properties of the complex, is not unprecedented. A study[44] carried out on a series of complexes with the formula $[Fe(PY5)(Y)]^{n+}$, where PY5 = 2,6-(bis(bis-2-pyridyl)-methoxymethane)pyridine and Y represents a series of neutral and anionic exogenous monodentate ligands, revealed that the MeOH ligand in $[Fe(PY5)(MeOH)]^{n+}$ can be displaced by the addition of a Lewis base and that the anionic ligands enhance the reversibility of the $Fe^{II/III}$ redox reaction on Pt disk electrodes.

Photovoltaic Performance. Two new electrolytes based on redox shuttles, **2a**/**2b** and **3a**/**3b**, were optimized and tested for their performance in DSCs and compared to a standard electrolyte employing $[Co(bpy)_3]^{2+/3+}$ as redox couple. An

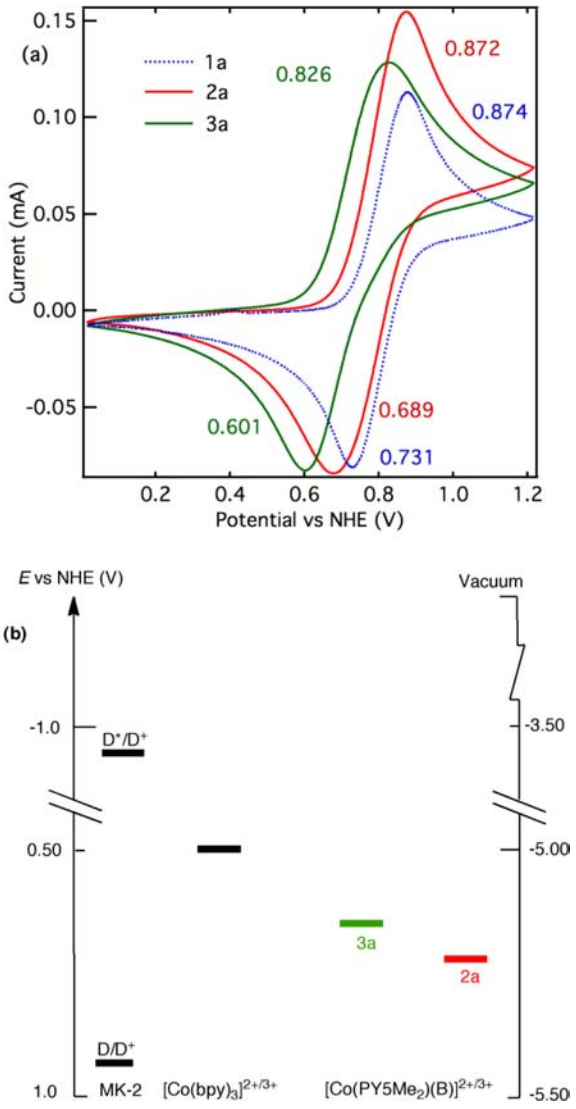

Figure 3. Cyclic voltammetry and energy level diagram. (a) Cyclic voltammogram of 10 mM solutions of $[Co(PY5Me_2)(MeCN)](OTf)_2$ in MeCN (blue wave 1), with 10 mM tBP added (red wave **2a**) and 10 mM NMBI added (green wave **3a**). The measurements were performed with use of a glassy carbon disk electrode and 100 mM $(Bu_4N)PF_6$ as supporting electrolyte at a scan rate of 100 mV/s. (b) Energy level diagram of DSC components, approximate redox potentials of the electrolytes[7] based on $[Co(bpy)_3]^{2+/3+}$ and complexes **2a** and **3a**. Data for MK2 dye and cobalt complexes are relative to the normal hydrogen electrode (NHE).

efficient, commercially available carbazole dye, MK2, was used as the photosensitizer. The redox potential (0.92 V versus NHE) of MK2 was measured on ITO films in acetonitrile containing 0.10 M $TBAPF_6$ as supporting electrolyte. The dye has a high molar extinction coefficient (38 400 M^{-1} cm^{-1})[49] and ensures excellent light harvesting, even when adsorbed onto relatively thin (2−5 μm) TiO_2 films. It is therefore a convenient sensitizer for DSCs based on one-electron-transfer redox couples, where the use of thinner than usual TiO_2 film thicknesses is preferred due to increased charge recombination as compared to I^-/I_3^-.

The highest energy conversion efficiency of 8.4% under simulated sunlight (AM 1.5 G, 1000 W/m^2) was achieved by using an electrolyte based on redox couple **3a**/**3b** (see Table

dx.doi.org/10.1021/ja305897k | J. Am. Chem. Soc. 2012, 134, 16646−16653

Table 3. Tabulated Photovoltaic Performance Data of DSCs Made with Different Redox Mediators and MK2 Dye under Simulated Sunlight (AM 1.5 G, 1000 W/m^2)[a]

redox couple	2a/b	3a/b	$[Co(bpy)_3]^{2+/3+}$	$[Co(bpy)_3]^{2+/3+}$
base[b]	tBP	NMBI	tBP	NMBI
RP (mV)[c]	684	633	496	498
V_{OC} (mV)	993 ± 2	940 ± 1	802 ± 1	795 ± 1
J_{SC} (mA cm^{-2})	8.1 ± 0.01	11.8 ± 0.4	14.1 ± 0.2	13.0 ± 0.3
FF	0.76 ± 0.01	0.77 ± 0.01	0.66 ± 0.01	0.67 ± 0.01
η (%)	6.1 ± 0.1	8.4 ± 0.3	7.4 ± 0.1	7.0 ± 0.2

[a]Double-layer TiO_2 films (1 μm mesoporous TiO_2 (30 nm) and 2 μm scattering TiO_2 (400 nm)) were used for the construction of all DSCs. A 0.5 μm thick PEDOT was used as counter electrode, which was grown electrochemically on FTO, using a 20 mM solution of EDOT monomer in acetonitrile and 100 mM LiTFSI as supporting electrolyte. The average performance values and standard deviation over a sample of three cells is given. [b]The electrolyte consists of 0.20 M Co^{II} complex, 0.075 M Co^{III} complex, 0.10 M LiTFSI, and 0.50 M of either tBP or NMBI as indicated. [c]The redox potential of the electrolytes were determined from the potential difference between a Pt wire and a reference electrode (Ag/Ag^+), immersed in the electrolyte.[7]

3). These DSCs clearly outperform devices based on the more conventional $[Co(bpy)_3]^{2+/3+}$ redox couple. The efficiency gain is primarily due to a significant increase in V_{OC} and fill factor (FF), which compensate for a drop in short-circuit current density (J_{SC}). The interpretation of changes in V_{OC} and J_{SC} for these cells is not straightforward, as the added bases influence the electronic properties of the mesoporous TiO_2 electrode (e.g., flat band position, surface states), while also creating different redox mediators through in situ reactions with **1a**/**1b**. The more positive redox potential of electrolytes based on **2a**/**2b** relative to $[Co(bpy)_3]^{2+/3+}$ is reflected in a higher V_{OC} of 993 mV for devices made with electrolytes containing **2a**/**2b**.

The performance of DSCs based on $Co^{II/III}$ polypyridyl electrolytes is highly dependent on the mesostructure of the TiO_2 film used to construct the cells. In this study, the TiO_2 films have been optimized for the use of MK2 in conjunction with $[Co(bpy)_3]^{2+/3+}$ based electrolytes (see the Experimental Section), yielding efficiencies (η) of up to 7.4%. This represents a substantial improvement over the 5.5% efficiency reported recently for DSCs based on MK2 and $[Co(bpy)_3]^{2+/3+}$ electrolyte.[45] Again, the key point to make here is that sensitizers with very high molar extinction coefficients are ideal for one-electron redox mediators, as a very thin film of 1 μm transparent TiO_2 nanoparticles is sufficient to ensure efficient light harvesting.

The IV curves for the best performing DSCs for each redox couple are shown in Figure 4, measured at AM1.5 G; 1000 W/m^2. The devices made with the NMBI complex, **3**, show a 140 mV higher V_{OC} and a significant increase in FF compared to devices employing a $[Co(bpy)_3]^{2+/3+}$ electrolyte. The 140 mV gain in V_{OC} is primarily attributed to the differences in the redox potentials[7] of the two electrolytes.

The measured redox potential for the $[Co(bpy)_3]^{2+/3+}$ electrolyte was in very close agreement with the standard Nernst potential calculated by Grätzel et al. for $[Co(bpy)_3]^{2+/3+}$ at very similar concentrations.[46] The lower J_{SC} values for devices based on **2a**/**2b** could be a consequence of less efficient dye-regeneration, and may arise from the lower driving force for this reaction (0.24 V). Photocurrent dynamics measurements, using simple on/off experiments (see Figure S5 in the SI), revealed that the photocurrents at 1 sun were somewhat limited by mass-transport limitations. This effect was slightly more pronounced for devices based on **3a**/**3b** compared to $[Co(bpy)_3]^{2+/3+}$. Inefficient dye regeneration could result in a significantly higher equilibrium concentration of photooxidized dye and therefore a faster rate of recombination between

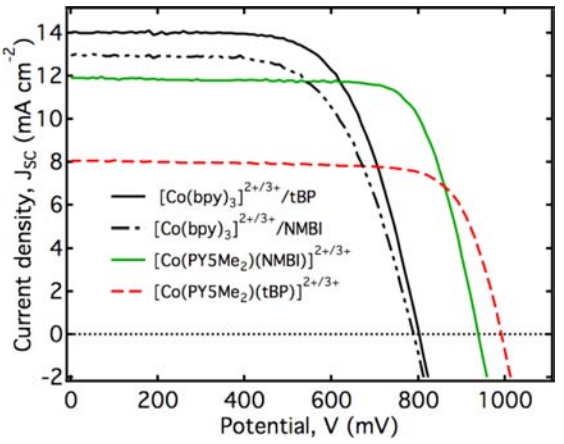

Figure 4. Comparison of DSC performance for optimized devices sensitized with MK2 based on **3a**/**3b** (green line), **2a**/**2b** (red dashed), $[Co(bpy)_3]^{2+/3+}$/tBP (black solid), and $[Co(bpy)_3]^{2+/3+}$/NMBI (black dotted) electrolytes in acetonitrile. IV characteristics are summarized in Table 3.

conduction band electrons and photooxidized dye molecules. In the future, we intend to investigate the electron transfer processes limiting the performance of these devices.

The incident photon-to-electron conversion efficiency (IPCE) spectra of DSCs sensitized with MK2 are shown in Figure 5. Comparable IPCEs are observed for the devices fabricated by using $[Co(bpy)_3]^{2+/3+}$ with either tBP or NMBI added as Lewis base. The devices fabricated with electrolytes based on complexes **2a**/**2b** and **3a**/**3b** show lower IPCEs compared to DSCs constructed from $[Co(bpy)_3]^{2+/3+}$ electrolytes. This is anticipated from the lower J_{SC} values measured under simulated sunlight (see Table 3).

IMVS-IMPS Spectroscopy. Further insights into the electron lifetime and mean transient time of photoinjected charge carriers were gained by using the intensity-modulated photovoltage and photocurrent spectroscopy (IMVS and IMPS), as complemented by charge extraction experiments. Figure 6a shows the IMPS results, which compare mean electron transient times (τ_c) as a function of J_{SC}. The observed τ_c for the devices based on redox systems **2a**/**2b**, **3a**/**3b**, and $[Co(bpy)_3]^{2+/3+}$ with tBP and NMBI are similar, as expected. It can be seen in Figure 6b that for each of the electrolyte systems, linear plots for electron lifetime measurements (τ_n) vs electron density were observed.

dx.doi.org/10.1021/ja305897k | J. Am. Chem. Soc. 2012, 134, 16646−16653

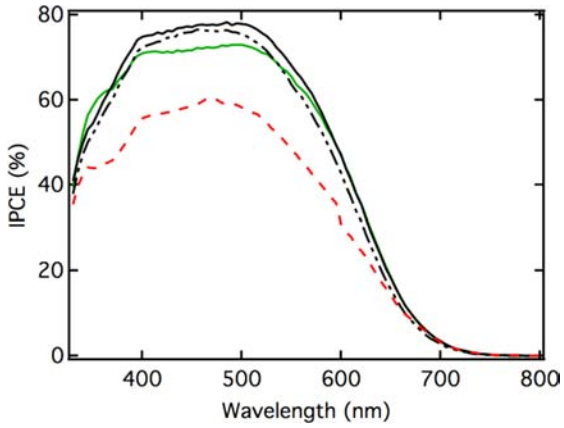

Figure 5. IPCE spectra for the DSCs sensitized with MK2 based on **3a**/**3b** (green line), **2a**/**2b** (red dashed), $[Co(bpy)_3]^{2+/3+}$/tBP (black solid), and $[Co(bpy)_3]^{2+/3+}$/NMBI (black dotted) electrolytes in acetonitrile.

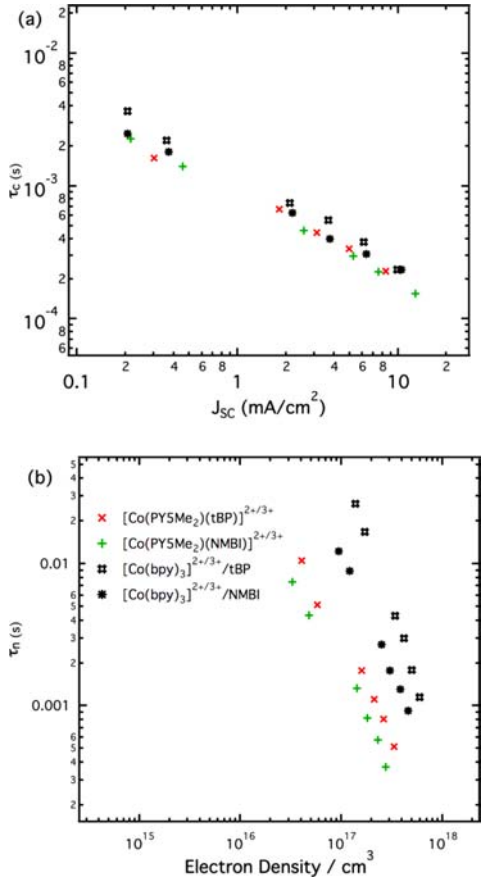

Figure 6. IMVS and IMPS spectroscopy. (a) Mean electron transient time versus short circuit current. (b) Electron lifetimes are plotted vs extracted charge for MK2-sensitized DSCs. The devices were constructed with use of 2 μm thick TiO_2 (30 nm) mesoporous films and contained the corresponding redox shuttle in their electrolyte. The electrolyte composition is given in Table 3.

The results are consistent with recombination occurring via electron transfer from the conduction band[47] to the oxidized form of the redox couple, despite large differences in the redox potentials of electrolytes as well as different reorganizational energies of the cobalt complexes. In general, faster electron transfer rates associated with redox systems based on complexes **2a**/**2b** and **3a**/**3b** can result in comparatively short electron lifetimes for photoinjected charge carriers. In contrast, the high-energy activation barrier relative to the $[Co(bpy)_3]^{2+/3+}$ redox couple brings about a 10-fold improvement in the lifetime of photoinjected charge carriers, at a similar charge density.

The classical inner-sphere reorganization energy associated with electron-exchange reactions of metal complexes can be estimated by the following equation:[41]

$$\Delta G_{inner} = \frac{n}{2}\frac{f_{III}f_{II}}{f_{III}+f_{II}}\Delta X^2$$

where f_i = force constants for the Co^{II} and Co^{III}-ligand bonds and ΔX = change in bond distances of n bonds. Assuming f_i and n to be similar for the $[Co(PY5Me_2)(NMBI)]^{2+/3+}$ (**3a**/**3b**) and $[Co(bpy)_3]^{2+/3+}$ redox couples, the estimated inner-sphere reorganizational energy varies with the square of the displacement. Compared with $[Co(bpy)_3]^{2+/3+}$ (where ΔX = 0.20 Å), a decrease in inner-sphere reorganizational energy of almost 50% is predicted for **3a**/**3b** (for which ΔX = 0.15 Å).[42,43] This is expected to result in faster dye regeneration but also in faster recombination between injected electrons and the oxidized redox mediator. Faster recombination for electrolytes with higher redox potentials is also expected as the driving force for dye regeneration is decreased for electron transfer processes operating in the Marcus normal region.[26] According to Hupp et al.[48] the open-circuit quasi-Fermi level drops (becomes less negative) with a positive increase in the redox potential of the redox couple and, hence, it reduces the attainable V_{OC}.

CONCLUSIONS

We have explored the application of a new class of redox mediators based on the complex $[Co(PY5Me_2)(MeCN)]^{2+/3+}$, where $PY5Me_2$ is a pentapyridyl ligand. Using a number of techniques, including X-ray crystallography, we have demonstrated that the MeCN ligand can be replaced by a more strongly binding monodentate ligand. Thus, the use of a pentadentate ligand allows the potential of the $Co^{II/III}$ redox couple to be tuned through the single-site coordination of tBP or NMBI, two Lewis bases commonly added to DSC electrolytes. Metal complexes based on the pentadentate ligand are also predicted to result in a lower reorganizational energy for electron transfer when compared to the $[Co(bpy)_3]^{2+/3+}$ redox couple. Application of electrolytes based on the cobalt-NMBI complexes in DSCs, in combination with a strongly absorbing organic sensitizer, MK2, have yielded devices with efficiencies of 9.2% and 8.4% at 0.1 and 1 sun irradiation, respectively, outperforming analogous devices constructed with the $[Co(bpy)_3]^{2+/3+}$ redox couple. In addition, an open circuit voltage approaching 1.0 V was measured for devices based on the tBP complexes **2a**/**2b**, as a consequence of the higher redox potential of this redox couple.

The ability of complexes, such as **1a**, to react with monodentate ligands opens a new avenue in DSC electrolyte research. That is, fine-tuning of the redox potential of the electrolyte through the judicious choice of the Lewis base. Moreover, complexes like **1a** are ideal model compounds for fundamental studies of recombination kinetics,[47] since different reaction driving forces can be achieved through the addition of appropriate ligands with little change in reorganization energy.

dx.doi.org/10.1021/ja305897k | J. Am. Chem. Soc. 2012, 134, 16646−16653

■ ASSOCIATED CONTENT

Supporting Information

Cyclic voltammogram for complexes **1a, 2a** and **3a**; electronic spectra for complexes **2a/b** and **3a/b**; crystal structure of complex **3b**, and cif files for complexes **2a**, **3a** and **3b**; pulsed light current transients for **3a/3b** and $[Co(bpy)_3]^{2+/3+}$; photovoltaic performance data at different light intensities for the devices made with **3a/3b**; and IMVS-IMPS spectroscopy of the cells made with complexes **2a/2b**, **3a/3b**, and $[Co(bpy)_3]^{2+/3+}$. This material is available free of charge via the Internet at http://pubs.acs.org.

■ AUTHOR INFORMATION

Corresponding Author

leone.spiccia@monash.edu; udo.bach@monash.edu

Notes

The authors declare no competing financial interest.

■ ACKNOWLEDGMENTS

Financial support from the Australian Research Council through the Discovery, Australian Research Fellowship and LIEF programs, the Commonwealth Scientific and Industrial Research Organization (Australia), the Australian Solar Institute, the Victorian State Government Department of Primary Industry (SERD Program, Victorian Organic Solar Cells Consortium), and Monash University is gratefully acknowledged. Valuable discussions with Torben Daeneke are gratefully acknowledged. This work was performed in part at the Melbourne Centre for Nanofabrication, an initiative partly funded by the Commonwealth of Australia and the Victorian Government. Work at Berkeley was supported by NSF Grant CHE-1111900 (J.R.L.), DOE/LBNL Grant 403801 (C.J.C.), and an NSF Graduate Research Fellowship (J.C.A.).

■ REFERENCES

(1) Zhang, C.; Dai, J.; Huo, Z.; Pan, X.; Hu, L.; Kong, F.; Huang, Y.; Sui, Y.; Fang, X.; Wang, K.; Dai, S. *Electrochim. Acta* **2008**, *53*, 5503.

(2) Nakade, S.; Makimoto, Y.; Kubo, W.; Kitamura, T.; Wada, Y. *J. Phys. Chem B* **2005**, *109*, 3488.

(3) Fabregat, F. S.; Bisquert, J. *Sol. Energy Mater. Sol. Cells* **2005**, *87*, 117.

(4) Krüger, J.; Plass, R.; Cevey, L.; Piccirelli, M.; Grätzel, M. *Appl. Phys. Lett.* **2001**, *2085*, 10.

(5) Nakade, S.; Kanzaki, T.; Kubo, W.; Kitamura, T.; Wada, Y.; Yanagida, S. *J. Phys. Chem B* **2005**, *109*, 3480.

(6) Bach, U.; Tachibana, Y.; Moser, J.-E.; Haque, S. A.; Durrant, J. R.; Grätzel, M.; Klug, D. R. *J. Am. Chem. Soc.* **1999**, *121*, 7445.

(7) Boschloo, G.; Haeggman, L.; Hagfeldt, A. *J. Phys. Chem B* **2006**, *110*, 13144.

(8) Huang, S. Y.; Schlichtho, G.; Nozik, A. J.; Grätzel, M.; Frank, A. J. *J. Phys. Chem B* **1997**, *101*, 2576.

(9) Nazeeruddin, M. K.; Kay, A.; Mueller, E.; Liska, P.; Vlachopoulos, N.; Grätzel, M. *J. Am. Chem. Soc.* **1993**, *115*, 6382.

(10) Kusama, H.; Orita, H.; Sugihara, H. *Langmuir* **2008**, *24*, 4411.

(11) Daeneke, T.; Uemura, Y.; Duffy, N. W.; Mozer, A. J.; Koumura, N.; Bach, U.; Spiccia, L. *Adv. Mater.* **2012**, *24*, 1222.

(12) Daeneke, T.; Kwon, T.-H.; Holmes, A. B.; Duffy, N. W.; Bach, U.; Spiccia, L. *Nature Chem.* **2011**, *3*, 211.

(13) Daeneke, T, A.; Mozer, A. J.; Kwon, T.-H.; Holmes, A. B.; Duffy, N. W.; Bach, U.; Spiccia, L. *Energy Environ. Sci.* **2012**, *5*, 7090.

(14) Bai, Y.; Yu, Q.; Cai, N.; Wang, Y.; Zhang, M.; Wang, P. *Chem. Commun.* **2011**, *47*, 4376.

(15) Teng, C.; Yang, X.; Yuan, C.; Li, C.; Chen, R.; Tian, H.; Li, S.; Hagfeldt, A.; Sun, L. *Org. Lett.* **2009**, *11*, 5542.

(16) Liu, J.; Zhang, J.; Xu, M.; Zhou, D.; Jing, X.; Wang, P. *Energy Environ. Sci.* **2011**, *4*, 3021.

(17) Tian, H.; Yu, Z.; Hagfeldt, A.; Kloo, L.; Sun, L. *J. Am. Chem. Soc.* **2011**, *133*, 9413.

(18) Rowley, J. G.; Farnum., H. B.; Ardo, S.; Meyer, J.G. . *J. Phsy. Chem. Lett.* **2010**, *1*, 3132.

(19) Yum, J.-H.; Baranoff, E.; Kessler, F.; Moehl, T.; Ahmad, S.; Bessho, T.; Marchioro, A.; Ghadiri, E.; Moser, J.-e.; Yi, C.; Nazeeruddin, K.; Grätzel, M. *Nature Commun.* **2012**, *3*, 631.

(20) Wang, M.; Chamberland, N.; Breau, L.; Humphry-baker, R.; Zakeeruddin, S. M.; Grätzel, M. *Nature Chem.* **2010**, *2*, 385.

(21) Cheng, M.; Yang, X.; Li, S.; Sun, L. *Energy Environ. Sci.* **2012**, *5*, 6290.

(22) Liu, J.; Zhang, J.; Xu, M.; Zhou, D.; Wang, P. *Energy Environ. Sci.* **2011**, *4*, 3021.

(23) Bai, Y.; Zhang, J.; Zhou, D.; Wang, Y.; Zhang, M.; Wang, P. *J. Am. Chem. Soc.* **2011**, *133*, 11442.

(24) Feldt, S. M.; Wang, G.; Boschloo, G.; Hagfeldt, A. *J. Phys. Chem. C* **2011**, *115*, 21500.

(25) Kavan, L.; Yum, J.-H.; Grätzel, M. *Nano Lett.* **2011**, *11*, 5501.

(26) Feldt, S. M.; Gibson, E. A.; Gabrielsson, E.; Sun, L.; Boschloo, G.; Hagfeldt, A. *J. Am. Chem. Soc.* **2010**, *132*, 16714.

(27) Cazzanti, S.; Caramori, S.; Argazzi, R.; Elliott, C. M.; Bignozzi, C. A.; Chimica, D.; Borsari, V. L. *J. Am. Chem. Soc.* **2006**, *128*, 9996.

(28) Moser, J. E.; Zakeeruddin, S. M.; Nazeeruddin, M. K.; Grätzel, M. *J. Phys. Chem. B* **2001**, *105*, 10461.

(29) Sapp, S. A.; Elliott, C. M.; Contado, C.; Caramori, S.; Bignozzi, C. A. *J. Am. Chem. Soc.* **2002**, *124*, 11215.

(30) Yella, a.; Lee, H.-W.; Tsao, H. N.; Yi, C.; Chandiran, a. K.; Nazeeruddin, M. K.; Diau, E. W.-G.; Yeh, C.-Y.; Zakeeruddin, S. M.; Grätzel, M. *Science* **2011**, *334*, 629.

(31) Hamann, T. W. *Dalton Trans.* **2012**, *41*, 3111.

(32) Weaver, M. J.; Yee, E. L. *Inorg. Chem.* **1980**, *19*, 1936.

(33) Sutin, N. *Acc. Chem. Res.* **1982**, *15*, 275.

(34) Marcus, R. A. *Annu. Rev. Phys. Chem.* **1964**, *15*, 155.

(35) Bechlars, B.; Alessandro, D. M. D.; Jenkins, D. M.; Iavarone, A. T.; Glover, S. D.; Kubiak, C. P.; Long, J. R. *Nature Chem.* **2010**, *2*, 362.

(36) Zadrozny, J. M.; Freedman, D. E.; Jenkins, D. M.; Harris, T. D.; Iavarone, A. T.; Mathoniere, C.; Clerac, R.; Long, J. R. *Inorg. Chem.* **2010**, *49*, 8886.

(37) Sheldrick, G. M. *Acta Crystallogr., Sect. A* **2008**, *64*, 112.

(38) Tsao, H. N.; Burschka, J.; Yi, C.; Kessler, F.; Nazeeruddin, M. K.; Grätzel, M. *Energy Environ. Sci.* **2011**, *4*, 4921.

(39) Sun, Y.; Bigi, J. P.; Piro, N. A.; Tang, M. L.; Long, J. R.; Chang, C. J. *J. Am. Chem. Soc.* **2011**, *133*, 9212.

(40) Karunadasa, H. I.; Chang, C. J.; Long, J. R. *Nature* **2010**, *464*, 1329.

(41) Endicott, J. F.; Brubaker, G. R.; Ramasami, T.; Kumar, K.; Dwarakanath, K.; Cassel, J.; Johnson, D. *Inorg. Chem.* **1983**, *22*, 3754.

(42) Yao, J.-C.; Ma, L.-F.; Yao, F-J. *Z. Kristallogr.—New Cryst. Struct.* **2005**, *220*, 483.

(43) Du, M.; Zhao, X.-J.; Cai, H. *Z. Kristallogr.—New Cryst. Struct.* **2004**, *219*, 463.

(44) Goldsmith, C. R.; Jonas, R. T.; Cole, A. P.; Stack, T. D. P. *Inorg. Chem.* **2002**, *41*, 4642.

(45) Kim, H.-S.; Ko, S.-B.; Jang, I.-H.; Park, N.-G. *Chem. Commun.* **2011**, *47*, 12637.

(46) Tsao, H. N.; Yi, C.; Moehl, T.; Yum, J.-H.; Zakeeruddin, S. M.; Nazeeruddin, M. K.; Grätzel, M. *ChemSusChem* **2011**, *4*, 591.

(47) Ondersma, J. W.; Hamann, T. W. *J. Am. Chem. Soc.* **2011**, *133*, 8264.

(48) Devries, M. J.; Pellin, M. J.; Hupp, J. T. *Langmuir* **2010**, *26*, 9082.

(49) Wang., Z.-S.; Koumura., N.; Cui., Y.; Takahashi, M.; Sekiguchi., H.; Mori., A.; Kubo., T.; Furube., A.; Hara., K. *Chem. Mater.* **2008**, *20*, 3993.